Quantifying the accuracy and precision of a novel real-time 6 degree-of-freedom kilovoltage intrafraction monitoring (KIM) target tracking system

J-H Kim[1], D T Nguyen[1], C-Y Huang[1], T Fuangrod[2], V Caillet[1,4], R O'Brien[1], P Poulsen[3], J Booth[4,5] and P Keall[1]

[1] Faculty of Medicine, The University of Sydney, Sydney, Australia

[2] Department of Radiation Oncology, Calvary Mater Hospital, Newcastle, Australia

[3] Department of Oncology, Aarhus University Hospital, Aarhus, Denmark

[4] Royal North Shore Hospital, St Leonards, Australia

[5] School of Physics, University of Sydney, Sydney, Australia

Corresponding author : Jung-Ha Kim jung.kim@sydney.edu.au

Acknowledgments

This project is supported by a Cancer Australia (1085360) grant.

Abstract

Target rotation can considerably impact the delivered radiotherapy dose depending on the tumour shape. More accurate tumour pose during radiotherapy treatment can be acquired through tracking in 6 degrees-of-freedom (6 DoF) rather than in translation only. A novel real-time 6 DoF kilovoltage intrafraction monitoring (KIM) target tracking system has recently been developed. In this study, we experimentally evaluated the accuracy and precision of the 6 DoF KIM implementation. Real-time 6 DoF KIM motion measurements were compared against the ground truth motion retrospectively derived from kV/MV triangulation for a range of lung and prostate tumour motion trajectories as well as for various static poses using a phantom. The accuracy and precision of 6 DoF KIM were calculated as the mean and standard deviation of the differences between KIM and kV/MV triangulation for each DoF, respectively. We found that KIM is able to provide 6 DoF motion with sub-degree and sub-millimetre accuracy and precision for a range of realistic tumour motion.

1. Introduction

Real-time tumour motion adaptive radiation therapy is of an increasing interest for more accurate delivery of radiation doses to tumour in the presence of moving and deforming anatomy. At present, intrafraction tumour motion is accounted for by 'gating', which allows delivery of the treatment within a defined motion range (Ohara et al 1989, Berbeco et al 2005, Smith et al 2009, Keall et al 2015) or by 'tracking', which continuously delivers the treatment by dynamically shifting MLC aperture according to the three-dimensional (3D) tumour position (Neicu et al 2003, Keall et al 2014), or by dynamically repositioning the x-ray beam and target alignment (Adler et al 1999, D'Souza et al 2005, Depuydt et al 2014). Both these techniques require accurate real-time localisation of the tumour.

Several methods have been clinically implemented to monitor intrafraction tumour motion in real-time, based on the use of markers, e.g. electromagnetic transponders (Balter et al 2003), implanted near the tumour, or the use of imaging modalities, e.g. fluoroscopy (Shirato et al 2000). For respiratory motion, lung volume spirometer, or external optical markers are used to measure abdominal displacement as a surrogate (Bowen et al 2012).

Many previous studies demonstrated non-negligible rotational tumour motion (Huang et al 2014, Bertholet et al 2016) during the treatment, which could lead to significant underdosing even if the translation tumour motion was managed (Deutschmann et al 2012, Amro et al 2013, de Boer et al 2015). Appropriate management of the rotational tumour motion can further reduce the treatment margins by more than 4 mm (Li et al 2009), while still assuring target coverage.

Real-time monitoring of six degrees-of-freedom (6 DoF) tumour motion using kilovoltage intrafraction monitoring (KIM) was developed (Tehrani et al 2013), which was used to retrospectively quantify the 6 DoF motion of prostate (Huang et al 2014) and liver cancer patients (Bertholet et al 2016). Recently, this method was clinically implemented for the first time for real-time use in a pilot trial and the TROG 15.01 SPARK trial (Nguyen et al 2017). The SPARK trial has the aim of collecting the real-time measurement of 6 DoF intrafraction tumour motion from a cohort of 48 prostate cancer patients. However, the accuracy of the 6 DoF

motion estimation by this method has only been evaluated in simulations for a known rotation (Tehrani et al 2013) and has not yet been quantified experimentally.

As a first step towards real-time 6 DoF tumour motion adaptive radiotherapy, this study aims to quantitatively evaluate the accuracy and precision of the real-time 6 DoF motion estimates by comparison with ground truth motion derived using kV/MV triangulation.

2. Methods

Conventional KIM determines the three-dimensional (3D) position of implanted markers in real-time during radiotherapy using a series of kilovoltage (kV) projections acquired by a gantry-mounted kV x-ray imager with sub-millimetre accuracy (Keall et al 2015). Recently, an extension to this technique has been made by implementing an iterative closest point (ICP) algorithm (Umeyama 1991), enabling the transition from 3D to 6 DoF monitoring of intrafractional tumour motion (Tehrani et al 2013). The ICP algorithm iteratively estimates the transformation from the set of target and source marker positions by minimising the root mean square distance between target and rigidly transformed source positions as the cost function. Six parameters describing three translations and three rotations about the left–right (LR), superior–inferior (SI) and anterior–posterior (AP) axes, are used to represent the rigid transformation in 6 DoF, and these are denoted as T_{LR}, T_{SI}, T_{AP}, R_{LR}, R_{SI}, R_{AP}, respectively. The accuracy and precision of 6 DoF KIM motion measurements were quantitatively evaluated for a range of static poses and dynamic 6 DoF tumour motion trajectories, using a phantom.

2.1. Data acquisition

2.1.1. Experimental setup.

Real-time 6 DoF motion measurements were carried out with a clinical linear accelerator (Trilogy, Varian Medical Systems, Palo Alto, CA) equipped with a kV On-Board Imager. A thin layer of three gold fiducial markers that are currently used in KIM clinical trials (Keall et al 2015) were inserted in a custom-built phantom. The phantom was made of low-density material i.e. wood, to provide a good contrast for the markers in MV images facilitating the markers segmentation. The phantom was placed on a 5 DoF motion platform (HexaMotion™, Scandidos, Uppsala, Sweden), which is capable of executing time-varying 5 DoF motion of rotations about LR and SI-axes and translations in all three axes (R_{LR}, R_{SI}, T_{LR}, T_{SI}, T_{AP}) within its mechanical limits. The accuracy of this motion platform system was evaluated to be within 0.3 mm and 0.22° for translations and rotations, respectively (Cetnar et al 2016).

The motion platform was manufactured for its designated phantom (Delta4, Scandidos, Uppsala, Sweden), and calibrated to execute the motion relative to the centre of this phantom. The motion platform was modified in-house to allow the use of user specific phantoms similar to the method described in Ng et al (2014) and shown in figure 1. This modification caused an ambiguity in the origin (pivot) of the executed rotational motion and introduced an unknown offset between the centre of the phantom and the pivot of the motion platform, hence the input rotation to the platform could not be regarded as the phantom rotation. Therefore, the motion platform

only served to apply 5 DoF motion to the phantom, and not as the ground-truth. A standard treatment couch (Trilogy, Varian Medical Systems, Palo Alto, CA) was used to apply the static rotation in the remaining DoF (RAP). The experimental setup is shown in figure 1.

2.1.2. Radiation delivery.

A circular conformal arc field (7 cm in diameter) of 6 MV x-rays was delivered to the phantom with the gantry rotating from −140° to +140° (Varian IEC 601-2-1 scale) at 600 MUs min−1 using a Trilogy linear accelerator (Varian Medical Systems, Palo Alto, CA, US). During each arc beam delivery, various motion trajectories were applied to the phantom while kV and MV projections of the phantom were simultaneously acquired at 10 Hz with kV imaging parameters of 84 kVp, 50 mA and 4.0 ms. The images were live-streamed using a frame grabber cable to the iTools Capture software provided by Varian Medical Systems as described in Keall et al (2015).

2.1.3. Motion trajectories.

The phantom was initially positioned so that the centre of mass of the three markers coincided with the treatment isocentre. The 3D positions of the markers were estimated using KIM, which served as the reference pose for all subsequent measurements.

To test the accuracy of the system, firstly six static pose measurements were carried out by rotating the phantom to different static poses. A nominal rotation of ±2° about each axis was applied to the phantom for each arc, which differs from the actual rotation of the phantom due to the modification made to the motion platform as explained above. Then, a series of realistic 6 DoF motion trajectories were applied to the phantom to assess the accuracy of time-varying 6 DoF motion measurements. The realistic tumour motion trajectories were obtained from a previous study (Huang et al 2014) by retrospectively measuring the 6 DoF tumour motions for a number of lung and prostate fractions. The motion trajectories used in this study were the clinically-encountered lung and prostate tumour motion namely small, continuous, transient, persistent, high-frequency and erratic rotation for both tumour sites as reported in Huang et al (2014) (see figure 4 in Huang et al (2014)). A total of 6 static and 12 motion trajectories were investigated in the experiments.

2.1.4. Processing the motion trajectories for use with the motion platform.

The original lung and prostate motion trajectories could not be directly reproduced due to mechanical limitations of the motion platform. To overcome this limitation the following steps were taken to process the motion trajectories:

- Converting 6 DoF to 5 DoF by omitting R_{AP};
- Applying a scale factor on the motion if it exceeded the range of the platform;
- Applying a low-pass Butterworth filter with highest cutoff frequency (minimum filtering) required to be within the mechanical limit of the velocity and acceleration of the motion platform.

The minimal degree of scaling and filtering was applied to retain the realistic magnitude and pattern in the processed motion trajectories. Each processed trajectory was executed for each arc field. Examples of the original and processed motion trajectories are given as supplementary data.

2.2. 6 DoF motion acquisitions

Figure 2 shows the overall process to acquire the 6 DoF phantom motion used in this study. For all measurements with static and dynamic motion trajectories, the phantom motion in 6 DoF was measured in real-time using KIM and compared with the retrospectively derived ground truth motion from kV/MV triangulation.

2.2.1. Real-time 6 DoF KIM motion measurements.

KIM estimates 3D positions of the markers from 2D segmented markers positions on kV projections based on a probability density function (PDF) (Poulsen et al 2008b). In clinical application, kV images to estimate the PDF are collected during a gantry rotation prior to the treatment delivery (referred to as 'pre-treatment arc') to ensure accurate 3D marker position measurements during the entire treatment. In all our experiments, the collection of PDF data was incorporated into each measurement arc, where the first 20 s of the measurements were used to build a stable PDF, and therefore, succeeding 3D marker position estimates were regarded as analogous to the measurements during the treatment.

Based on the KIM reported 3D positions of the three markers, the 6 DoF motion was calculated on-the-fly using an ICP algorithm, which minimises the sum of squared differences between source (e.g. planned) and target (e.g. current) markers' positions (Tehrani et al 2013). These measurements were compared with the corresponding motion retrospectively derived from kV/MV triangulation.

2.2.2. Ground truth 6 DoF motion from kV/MV triangulation.

To assess the accuracy and precision of the 6 DoF motion measurements, the corresponding ground truth motion is required. In this study, we used the 6 DoF motion derived based on the 3D positions of the markers from the kV/MV triangulation as the ground truth. This technique has been used to benchmark the accuracy of 3D positional measurements using the KIM (Ng et al 2012, 2014, Keall et al 2015) since the kV/MV triangulation provides a concurrent measurement of the 3D positions of the same markers based on simultaneously acquired kV and MV stereoscopic images (Liu et al 2008). Based on the 3D triangulated positions of the markers, 6 DoF transformations between successive markers' positions can be calculated.

The main challenge in performing kV/MV triangulation is in marker segmentation in the MV images due to low contrast and marker occlusion by MLC leaves. This challenge was addressed by using a low-density phantom and open MV fields rather than VMAT. To minimise the observer's subjectivity and uncertainty in manual marker segmentation, the MV segmentation procedure was fully automated. In each MV frame, the intensity scale was inverted, and MLC shape was masked by applying a cutoff of 70% of the local intensity, which identified the in-field region of MLC aperture. A Laplacian of Gaussian (LoG) filter (Neycenssac 1993) with

varying standard deviation (σ) depending on the estimation of noise variance (Immerkær 1996) of the frame was applied. The markers in the frame were automatically detected by searching for the peak intensity within a region-of-interest of each marker defined based on the projected 3D KIM markers' positions at a given gantry angle.

Automatically segmented markers positions were visually inspected for all frames to eliminate incorrect segmentation. The 3D positions of the markers were then calculated by triangulating the segmented 2D positions of the markers on MV images with the corresponding positions from the kV images that were temporally synchronised with the MV images using the time stamps associated with each frame. Figure 3 is an example of the typical kV and MV images and segmented markers for the triangulation.

Based on the series of 3D triangulated markers' positions, the corresponding 6 DoF motion relative to the initial pose of the phantom was calculated using a closed-form least squares method to an absolute orientation problem (Horn 1987), which was chosen instead of the ICP algorithm for an independent derivation of the kV/MV 6 DoF motion. Since a minimum of three 3D points is required in the 6 DoF transformation calculations, only the frames with all three marker's 3D positions available were used to compute 6 DoF motion.

2.3. Quantifying the accuracy and precision of 6 DoF KIM-estimated motion.

The accuracy and precision of 6 DoF KIM motion were calculated as the mean and standard deviation (s.d.) of the differences compared with the corresponding 6 DoF motion derived by kV/MV triangulation in each DoF. As previously mentioned, the first 20 s arc was used for constructing the PDF of each marker for tracking, which was excluded from the analysis.

Further, it was also of interest to examine whether there is any relationship in the accuracy of the motion measurements on (i) the gantry angle; or (ii) the magnitude of the actual motion. This was assessed in each DoF individually by plotting the differences as a function of (i) the gantry angle (at which the corresponding MV frame was acquired); and (ii) the actual motion (the ground truth). The Pearson correlation coefficients in the actual motion (ground-truth) and the corresponding differences were also computed for dynamic tumour motion traces measurements.

3. Results

3.1. 6 DoF KIM versus 6 DoF kV/MV

3.1.1. Static poses.

Figure 4 compares the mean phantom rotations measured in real-time with 6 DoF KIM and retrospectively derived from kV/MV triangulation for different static rotations (±2° nominal) applied with the motion platform in SI and LR axes, and with rotating treatment couch in AP axis. As mentioned previously in section 2.1.1, the input motion of ±2° executed by the motion-platform, would differ from the actual phantom motion in isocentre coordinates due to an ambiguity in the origin of the motion platform's coordinate system caused by user-specific

modifications. Thus, the only comparable phantom motion in the same isocentre space are the KIM and kV/MV triangulation derived motions.

The mean and 1 s.d. of the measured phantom rotations are shown in figure 4 as the symbols and error bars, respectively. The mean of the real-time KIM measured rotations (red symbols) agreed with the corresponding ground truth (blue symbols) derived from the kV/MV triangulation in all axes to within 0.2°. The magnitudes of the error bars, which indicate the measurement uncertainties associated with each measurement, were comparable in the KIM and kV/MV measured rotation motions with the highest s.d. value of 0.33° and 0.37°, respectively.

3.1.2. Dynamic tumour motion traces.

Some typical examples of the time-varying 6 DoF tumour motion trajectories (erratic and transient) measured with KIM and the kV/MV triangulation are shown in figure 5. The mean and s.d. differences for each measurement are also displayed in each panel of the plots. It is shown that KIM and kV/MV measured 6 DoF motion traces agree well with the mean and s.d. differences all within 1° and 1 mm for rotations and translations, respectively.

3.2. Accuracy and precision of 6 DoF KIM measurements (mean and s.d. differences)

The mean and s.d. of differences for all measurements are summarized in table 1. The 6 DoF motion measured by KIM in real-time closely agreed with the corresponding ground-truth motion derived retrospectively from the KV/MV triangulation technique to within 1 mm and 1° for all tested motion types, except prostate transient trace where the s.d. differences were slightly larger than 1 mm in LR and 1° in SI directions. This particular motion trace was the one that required a high modification due to the limitations of the Hexamotion rotation ranges. This trace had the largest scaling factor was applied to R_{LR} reducing the peak R_{LR} motion from 16.7° down to 7.1° (See supplementary figure S1(b)). This may have caused a loss of motion fidelity, which could have adversely affected the accuracy of the KIM measurements.

The overall accuracy and precision of the 6 DoF KIM measurements slightly degraded for dynamic traces compared to static poses. This difference can be attributed to the increase in measurement uncertainty for the dynamic traces, due to (i) the effect of motion, which can causes blurring of the markers in both kV and MV images affecting the marker segmentation performance; and (ii) the effect of latency (less than 350 ms (Keall et al 2015)) causing the position differences between the real-time and retrospective measurements for dynamic motion measurements, which is not relevant for static measurements.

The box plot in figure 6 shows the median, 5% and 95% percentiles, and outliers of the differences in the calculated motion from the KIM and kV/MV triangulation in each DoF for different motion types applied. The median, 5% and 95% percentiles of the differences were all within 1 mm and 1° for all motion used in this study.

To assess any dependencies in the accuracy and precision of the KIM motion on gantry angles, the differences between KIM and kV/MV triangulated motion for all measurements were binned by approximately 3° gantry angle intervals, and the mean and s.d. differences were plotted (figure 7). KIM estimated translation in SI (T_{SI})

has relatively low differences from the ground truth. The T_{SI} motion is expected to be most accurate for the KIM since it can always be resolved irrespective to the gantry angle (Bertholet et al 2016).

The errors in TLR are expected to be larger at gantry angles of 0°, and decrease as gantry approaches 90° since LR motion is resolved in kV images at 0° gantry and unresolved in kV images at 90° gantry. A tendency of this behaviour is shown in the upper right panel of figure 7. An opposite behaviour is expected for T_{AP}, which was not clearly shown in the lower right panel of figure 7.

R_{LR} is determined by motion in the sagittal plane, i.e. in the SI and AP directions, therefore, is expected to be most accurate for lateral kV imaging (i.e. gantry at 0°). Such a trend is also seen in the upper left panel in figure 7. Similarly, R_{AP} is determined by motion in the coronal plane, i.e. in the SI and LR directions, thus it is expected to be most accurate for vertical kV imaging (i.e. gantry at ±90°) as shown in lower left panel.

Figure 8 shows the correlation plots with the calculated Pearson correlation coefficients (ρ) between the actual motion and the differences in each DoF. It appears as almost no correlations exist in the magnitude of error and the actual motion in almost all DoF ($\rho < 0.3$, except in TLR), which indicates that the accuracy and precision of 6 DoF motion measurements using KIM does not depend on the magnitude of the actual motion. A moderate correlation ($\rho = 0.47$) was found for translation in LR axis, which implies that the accuracy of KIM estimated LR motion to some extent depends on the magnitude of actual motion.

4. Discussion

Intrafractional tumour rotation could have a significant impact on delivered dose, particularly depending on tumour shape and isocentre placement. Recognising this, real-time 6 DoF tumour motion measurements during arc therapy have been enabled with KIM, and clinically implemented in a multicentre trial to provide valuable insight on the rotational as well as translational motion of the prostate tumour. It is of importance to validate the measured motion and maintain the accuracy of the measurements throughout the trial.

The ground truth 6 DoF motion in this study was obtained based on the kV/MV triangulation, which provides a concurrent measurement of the KIM estimated marker motion with no extra cost. In addition, given the collection of both kV and MV images during the treatment, the kV/MV 6 DoF motion measurements can accurately be obtained retrospectively for each patient treatment fraction. It should be noted that the accuracy of kV/MV triangulation depends on the accuracies of the synchronisation between kV and MV images, system calibration matrix, and marker segmentation. To reduce the uncertainty and subjectivity in marker segmentation, we have implemented an automatic MV marker segmentation method, which could be also applied to patient data.

A programmable motion platform capable of executing time-varying 5 DoF motion was used to apply the motion to the phantom. Combining it with a rotating treatment couch, the application of 6 DoF motion was realised.

The 6 DoF motion estimates from KIM and kV/MV triangulation were in excellent agreement with sub-millimetre and sub-degree mean and s.d. differences for the vast majority of the lung and prostate tumour motion trajectories as well as various static poses, assessed in this study. The largest differences were found for the measurements with the prostate transient motion trajectory with the s.d. differences slightly over 1.0°. This may be attributed to the loss of realistic shape in the applied motion, which is the basis of determining 3D positions from 2D positions of the markers in KIM, as a result of significant smoothing of the tumour motion trajectory in an attempt to meet the mechanical limits of the motion platform.

In addition, 3D markers positions are estimated in KIM based on the mean, s.d. positions of the markers as well as using the inter-axes correlations. In previous study, it was recommended not to optimise the LR motion for prostate based on the correlation (setting ρLR-SI and ρLR-SI to zero), as it is shown to be very small and not well-correlated with other axes (Poulsen et al 2008a). Since the LR motion is not being optimised with correlations to the other axes, the error is likely to increase depending on the magnitude of the motion, which is evident in figure 8.

The accuracy and precision of the 6 DoF KIM motion measurements appear to be independent of the magnitude of the actual motion (figure 8), however, it should be noted that the magnitude of the patient motion used in this study were relatively small: within 7° for rotations and 1 cm for translations. This was because in this study the magnitude of the motion was restricted mainly by the mechanical limitations associated with the motion platform and also the limitations in the 6 DoF tumour trajectories acquired from patients. A previous study (Poulsen et al 2008a) reported that the accuracy and precision of KIM motion measurements are independent of the magnitude of the actual motion, which included up to 56 mm translation motion in one axis. This implies that the results presented in this paper will not be affected for the larger magnitude of the motion, however, this hypothesis requires similar experimental validation to this study. The development of a 6 DoF motion platform with a larger range of motion and further acquisition of 6 DoF tumour motion trajectories could enable the assessment of larger motion ranges in the future.

In our experiments, an unknown offset between the centroid of the markers (which was aligned to coincide with the treatment isocentre at the start of the measurements) and the origin of the motion platform, introduced an increase in the magnitude of translations in LR direction to within ±1 mm in the processed input trajectory shown in figure S1 (b) to up to about 4 mm in the measured output with kV/MV triangulation as shown in figure 5(b). This has increased the error in LR direction to have up to 1 mm s.d., however, this could well not be present in the patient as this issue has risen from an attempt to meet the experimental limits—(i) processing the tumour trajectory; and (ii) offset between the applied motion to the centre of the markers. A follow-up study using the patient data will be carried out to provide further evidence on this effect.

The set of dynamic tumour motion experiments were repeated, which confirmed that the reproducibility of the accuracy and precision of 6 DoF KIM motion measurements to within 1° and 1 mm. The repeat experiments

were carried out with a time offset of 20 s to assess the effect of different motion phase, and the results showed that the accuracy and precision of KIM do not depend on the phase of the motion.

Several practical challenges are associated with clinically implementing the real-time 6 DoF KIM measurements. First, KIM tracks the implanted markers as a surrogate, and not the actual tumour. The target localisation error in practice, therefore, will also need to account for the distance between the surrogate (i.e. centroid of the markers) and the tumour (Bertholet et al 2016). Second, a minimum of three markers is required for 6 DoF motion estimation. The use of more markers is expected to increase the accuracy of the motion estimates, however, this assumption needs to be explored. Third, the arrangement of the implanted markers could impact the rotation motion measurements: e.g. a co-linear marker arrangement could degrade the rotation measurement accuracy. Although it is more unlikely to have the markers implanted in a completely co-linear geometry, the effect of the marker arrangement on the accuracy and precision of the 6 DoF KIM motion estimates remains to be investigated in the future.

Furthermore, there are other factors that could contribute to the final tumour localisation error in practice: As the 6 DoF motion describes the transformation of a rigid body, depending on the tumour sites (e.g. lung or liver), which undergo deformation, the accuracy of 6 DoF motion estimates could also be affected by the tumour deformation and marker migration. Previous studies have shown that the tumour deformations or marker migrations could falsely be interpreted as the tumour rotations (Wunderink et al 2010, Worm et al 2016), and the magnitudes of the errors resulting from tumour rotations and deformations are of the similar magnitude (Bertholet et al 2016).

This study validates the accuracy of the real-time 6 DoF KIM motion measurements in an experimental setting for the first time, which could be used as a routine QA of the 6 DoF KIM. In reverse, although it has not been assessed in this study, 6 DoF KIM could also be useful in commissioning a 6 DoF couch. This method can also be applied to the clinical data to ensure the accuracy of the acquired 6 DoF motion estimates acquired from the on-going clinical trial. A further assessment of the clinical data may reveal the true clinical impact of monitoring the tumour motion in 6 DoF.

5. Conclusions

Six DoF intrafractional tumour motion can be measured in real-time from 2D kV image projections using KIM with a sub-millimetre and sub-degree accuracy and precision for clinically realistic prostate and lung tumour motion during radiotherapy.

References

Adler J R, Murphy M J and Chang S D 1999 Image-guided robotic radiosurgery Neurosurgery 44 1299–306

Amro H, Hamstra D A, McShan D L, Sandler H, Vineberg K, Hadley S and Litzenberg D 2013 The dosimetric impact of prostate rotations during electromagnetically guided external-beam radiation therapy Int. J. Radiat. Oncol. Biol. Phys. 85 230–6

Balter J M, Wright N, Dimmer S, Friemel B, Newell J, Cheng Y and Mate T 2003 Demonstration of accurate localization and continuous tracking of implantable wireless electromagnetic transponders Int. J. Radiat. Oncol. Biol. Phys. 57 S264–5

Berbeco R I, Mostafavi H, Sharp G C and Jiang S B 2005 Towards fluoroscopic respiratory gating for lung tumours without radiopaque markers Phys. Med. Biol. 50 4481–90

Bertholet J, Worm E S, Fledelius W, Hoyer M and Poulsen P R 2016 Time-resolved intrafraction target translations and rotations during stereotactic liver radiation therapy: implications for marker-based localization accuracy Int. J. Radiat.Oncol. Biol. Phys. 95 802–9

Bowen S R, Nyflot M J, Gensheimer M, Hendrickson K R G, Kinahan P E, Sandison G A and Patel S A 2012 Challenges and opportunities in patient-specific motion managed and PET/CT-guided radiation therapy of lung cancer: review and perspective Clin. Transl. Med. 1 18

Cetnar A, James J and Wang B 2016 Commissioning of a motion systemt to investigate dosimetric consequences due to variability of respiratory waveforms J. Appl. Clin. Med. Phys. 17 283–92

D'Souza W D, Naqvi S A and Yu C X 2005 Real-time intra-fraction-motion tracking using the treatment couch: a feasibility study Phys. Med. Biol. 50 4021–33

de Boer J, Wolf A L, Szeto Y Z, van Herk M and Sonke J-J 2015 Dynamic collimator angle adjustments during volumetric modulated arc therapy to account for prostate rotations Int. J. Radiat. Oncol. Biol. Phys. 91 1009–16

Depuydt T et al 2014 Treating patients with real-time tumor tracking using the Vero gimbaled linac system: implementation and first review Radiother. Oncol. 112 343–51

Deutschmann H et al 2012 First clinical release of an online, adaptive, aperture-based image-guided radiotherapy strategy in intensity-modulated radiotherapy to correct for inter- and intrafractional rotations of the prostate Int. J. Radiat. Oncol. Biol. Phys. 83 1624–32

Horn B K P 1987 Closed-form solution of absolute orientation using unit quaternions J. Opt. Soc. Am. 4 629–42

Huang C-Y, Tehrani J N, Ng J A, Booth J and Keall P 2014 Six degrees-of-freedom prostate and lung tumor motion measurements using kilovoltage intrafraction monitoring Int. J. Radiat. Oncol. Biol. Phys. 91 368–75

Immerkær J 1996 Fast noise variance estimation Comput. Vis. Image Underst. 64 300–2

Keall P, Colvill E, O'Brien R, Ng J A, Poulsen P, Eade T, Kneebone A and Booth J 2014 The first clinical implementation of electromagnetic transponder-guided MLC tracking Med. Phys. 41 020702

Keall P J et al 2015 The first clinical treatment with kilovoltage intrafraction monitoring (KIM): a realtime image guidance method Med. Phys. 42 354–8

Li J S, Jin L, Pollack A, Horwitz E M, Buyyounouski M K, Price R A Jr and Ma C M 2009 Gains from real-time tracking of prostate motion during external beam radiation therapy Int. J. Radiat.Oncol. Biol. Phys. 75 1613–20

Liu W, Wiersma R D, Mao W, Luxton G and Xing L 2008 Real-time 3D internal marker tracking during arc radiotherapy by the use of combined MV–kV imaging Phys. Med. Biol. 53 7197–213

Neicu T, Shirato H and Seppenwoolde Y 2003 Synchronized moving aperture radiation therapy (SMART): average tumour trajectory for lung patients Phys. Med. Biol. 48 587

Neycenssac J 1993 Contrast enhancement using the Laplacian-of-a-Gaussian filter CVGIP, Graph. Models Image Process. 55 447–63

Ng J A, Booth J T, O'Brien R, Colvill E, Huang C-Y, Poulsen P R and Keall P J 2014 Quality assurance for the clinical implementation of kilovoltage intrafraction monitoring for prostate cancer VMAT Med. Phys. 41 111712

Ng J A, Booth J, Poulsen P, Fledelius W, Worm E, Eade T, Hegi F, Kneebone A, Kuncic Z and Keall P J 2012 Kilovoltage intrafraction monitoring for prostate intensity modulated arc therapy: first clinical results Int. J. Radiat. Oncol. Biol. Phys. 84 e655–61

Nguyen D T et al 2017 The first clinical implementation of a real-time six degree of freedom target tracking system during radiation therapy based on kilovoltage intrafraction monitoring (KIM) Radiotherp. Oncol. 123 37–42

Ohara K, Okumura T, Akisada T, Inada T, Mori T, Yokota H and Calguas M B 1989 Irradiation synchronized with respiration gate Int. J. Radiat. Oncol. Biol. Phys. 17 853–7

Poulsen P R, Cho B and Keall P J 2008a A method to estimate mean position, motion magnitude, motion correlation, and trajectory of a tumor from cone-beam CT projections for image-guided radiotherapy Int. J. Radiat. Oncol. Biol. Phys. 72 1587–96

Poulsen P R, Cho B, Langen K, Kupelian P and Keall P J 2008b Three-dimensional prostate position estimation with a single x-ray imager utilizing the spatial probability density Phys. Med. Biol. 53 4331–53

Shirato H et al 2000 Four-dimensional treatment planning and fluoroscopic real-time tumor tracking radiohterapy for moving tumor Int. J. Radiat. Oncol. Biol. Phys. 48 435–42

Smith R L, Lechleiter K, Malinowski K, Shepard D M, Housley D J, Afghan M, Newell J, Petersen J, Sargent B and Parikh P 2009 Evaluation of linear accelerator gating with real-time electromagnetic tracking Int. J. Radiat. Oncol. Biol. Phys. 74 920–7

Tehrani J N, O'Brien R, Poulsen P R and Keall P 2013 Real-time estimation of prostate tumor rotation and translation with a kV imaging system based on an iterative closest point algorithm Phys. Med. Biol. 58 8517

Umeyama S 1991 Least-squares estimation of transformation parameters between two point patterns IEEE Trans. Pattern Anal. Mach. Intell. 13 376–80

Worm E S, Bertholet J, Hoyer M, Fledelius W, Hansen A T, Larsen L P, Nielsen J E and Poulsen P R 2016 Fiducial marker guided stereotactic liver radiotherapy: is a time delay between marker implantation and planning CT needed? Radiother. Oncol. 121 75–8

Wunderink W, Romero M, Seppenwoolde Y, de Boer H, Levendag P and Heijmen B 2010 Potentials and limitations of guiding liver stereotactic body radiation therapy set-up on liver-implanted fiducial markers Int. J. Radiat. Oncol. Biol. Phys. 77 1573–83

Table 1. The mean (s.d.) differences of 6 DoF motion from KIM and kV/MV triangulations for various phantom motion tested in this study including static rotation poses and dynamic lung/prostate tumour motion trajectories.

Applied phantom motion			Rotations (°)			Translations (mm)		
			LR	SI	AP	LR	SI	AP
Static Poses	Tilt (R_{LR}) +2°		−0.15 (0.18)	0.06 (0.25)	0.06 (0.10)	0.07 (0.44)	−0.13 (0.05)	0.25 (0.16)
	Tilt (R_{LR}) −2°		0.02 (0.25)	0.02 (0.18)	−0.07 (0.10)	0.04 (0.44)	−0.04 (0.05)	−0.04 (0.16)
	Roll (R_{SI}) +2°		−0.12 (0.39)	0.06 (0.31)	−0.06 (0.16)	0.04 (0.39)	−0.04 (0.11)	−0.02 (0.41)
	Roll (R_{SI}) −2°		0.23 (0.21)	−0.10 (0.22)	−0.15 (0.10)	0.20 (0.12)	0.06 (0.05)	−0.29 (0.21)
	Yaw (R_{AP}) +2°		0.17 (0.21)	0.02 (0.17)	−0.16 (0.09)	0.23 (0.13)	0.07 (0.05)	−0.25 (0.23)
	Yaw (R_{AP}) −2°		−0.07 (0.16)	−0.05 (0.28)	0.06 (0.09)	0.09 (0.41)	−0.13 (0.05)	0.21 (0.17)
Dynamic trajectories	Prostate tumour motion	Continuous	−0.01 (0.31)	−0.14 (0.27)	0.01 (0.18)	0.02 (0.44)	0.12 (0.12)	0.40 (0.42)
		Erratic	0.12 (0.50)	−0.24 (0.54)	0.23 (0.20)	0.04 (0.41)	−0.07 (0.16)	0.44 (0.49)
		High Frequency	0.07 (0.14)	0.43 (0.70)	0.15 (0.56)	0.43 (0.70)	0.07 (0.39)	0.12 (0.18)
		Persistent	0.04 (0.22)	0.17 (0.20)	0.13 (0.13)	0.11 (0.36)	0.02 (0.10)	0.28 (0.35)
		Stable	0.13 (0.50)	−0.09 (0.27)	0.14 (0.15)	0.28 (0.62)	0.02 (0.12)	0.04 (0.64)
		Transient	−0.56 (0.68)	0.16 (1.04)	0.04 (0.41)	−0.62 (1.01)	0.08 (0.16)	0.92 (0.55)
	Lung tumour motion	Continuous	−0.16 (0.40)	0.24 (0.39)	0.23 (0.23)	−0.18 (0.97)	−0.08 (0.18)	−0.15 (0.72)
		Erratic	0.04 (0.54)	0.08 (0.52)	0.01 (0.20)	0.43 (0.44)	−0.08 (0.15)	0.64 (0.61)
		High Frequency	−0.09 (0.46)	0.05 (0.36)	0.44 (0.67)	0.31 (0.51)	−0.02 (0.12)	0.56 (0.50)
		Persistent	−0.10 (0.39)	0.35 (0.86)	0.11 (0.37)	0.16 (0.91)	0.06 (0.31)	0.37 (0.58)
		Stable	−0.05 (0.29)	0.16 (0.57)	0.19 (0.33)	0.02 (0.63)	−0.02 (0.23)	0.36 (0.44)
		Transient	0.11 (0.36)	0.14 (0.82)	−0.05 (0.20)	0.74 (0.57)	0.01 (0.27)	0.16 (0.80)

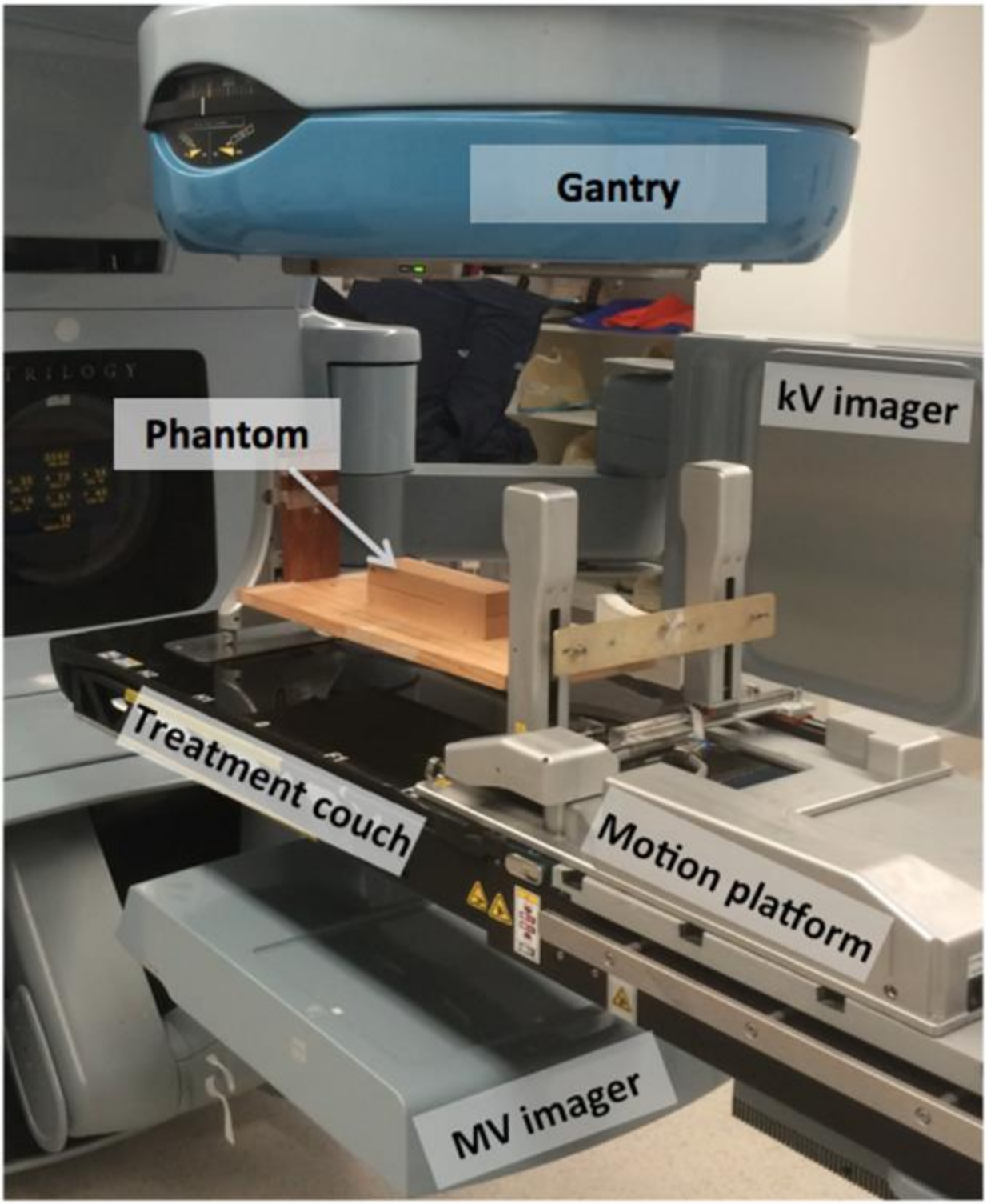

Figure 1. The experimental setup to measure the accuracy and precision of the 6 DoF KIM system: the custom-built phantom with three embedded gold markers sits on the modified motion platform placed on the treatment couch.

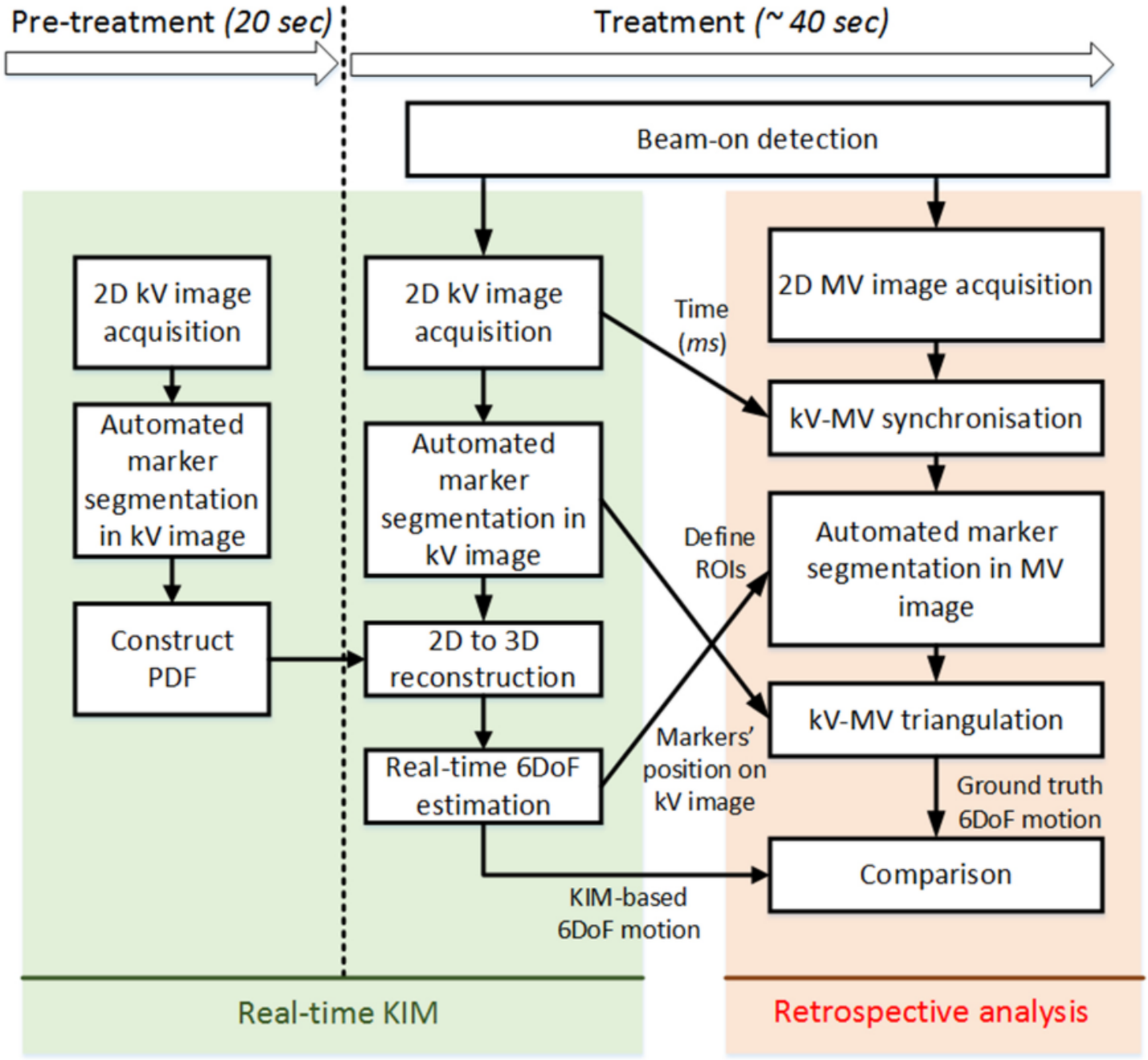

Figure 2. Workflow of the 6 DoF motion accuracy and precision measurements comparing KIM with kV/MV triangulation.

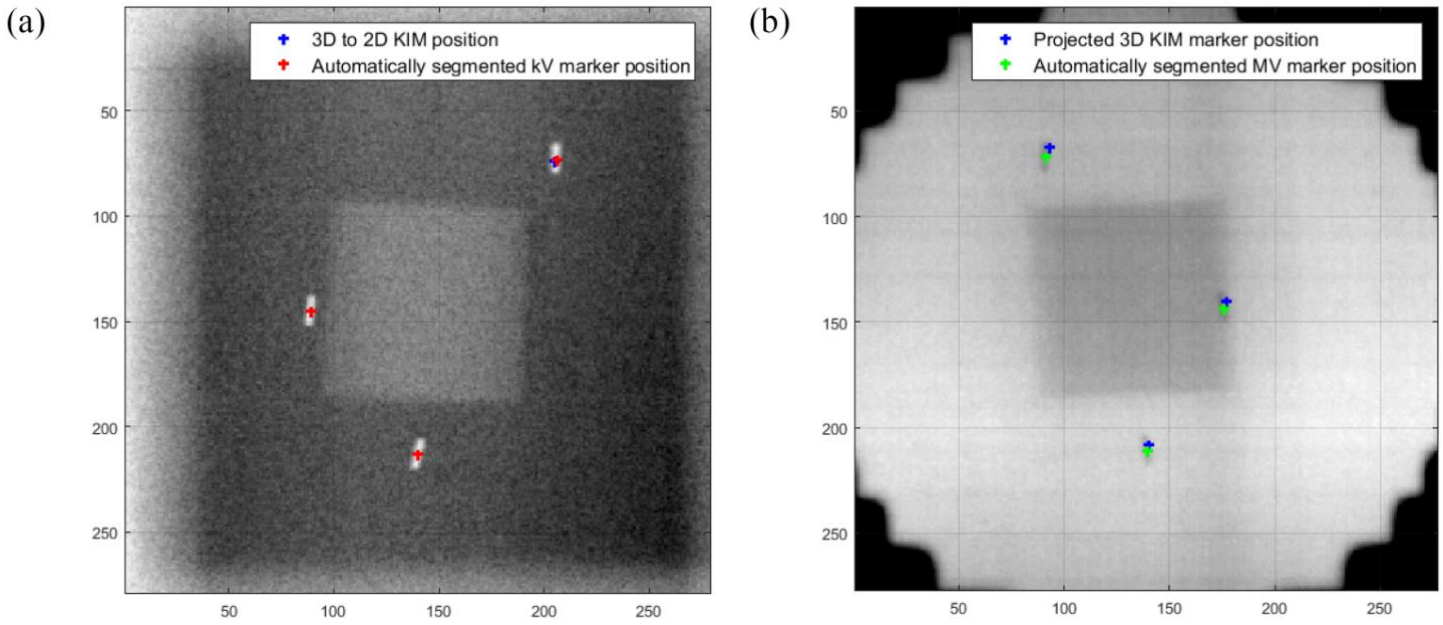

Figure 3. Corresponding kV (a) and MV (b) images of the phantom with three markers synchronised based on the time-stamps. Forward projected real-time KIM estimated 3D positional information is blue in both images (a) and (b); automatically segmented markers in kV images are in red and in MV images are in green crosses. (a) Synchronised kV image: (frame no. = 307; kV source angle = −142.6°) and (b) MV image: (frame no. = 270; Gantry angle = −52.6°).

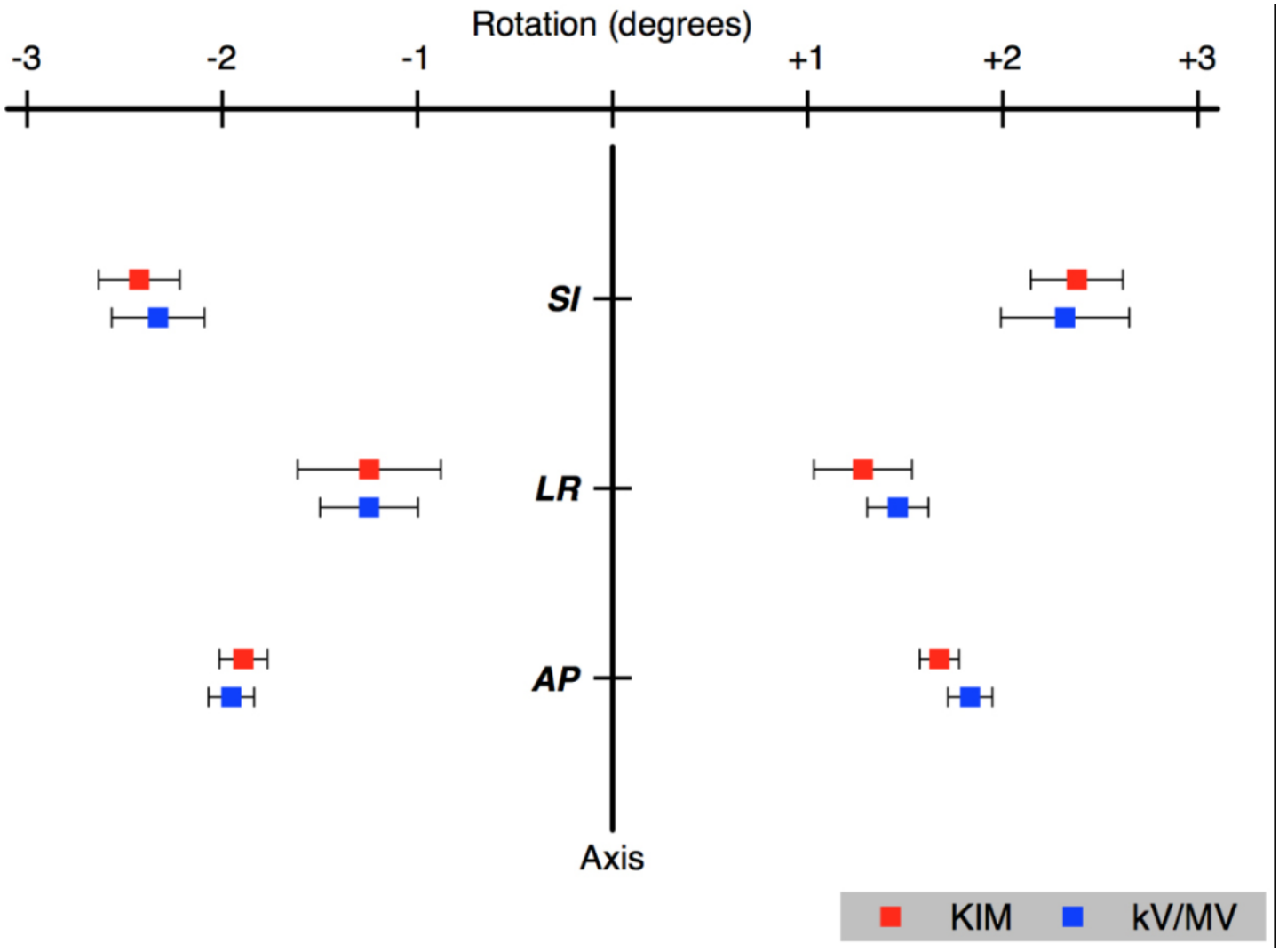

Figure 4. The mean rotations of the phantom estimated by KIM (red) and kV/MV (blue) for applied static rotations about each axis (i.e. static poses). Error bars are ±1 s.d.

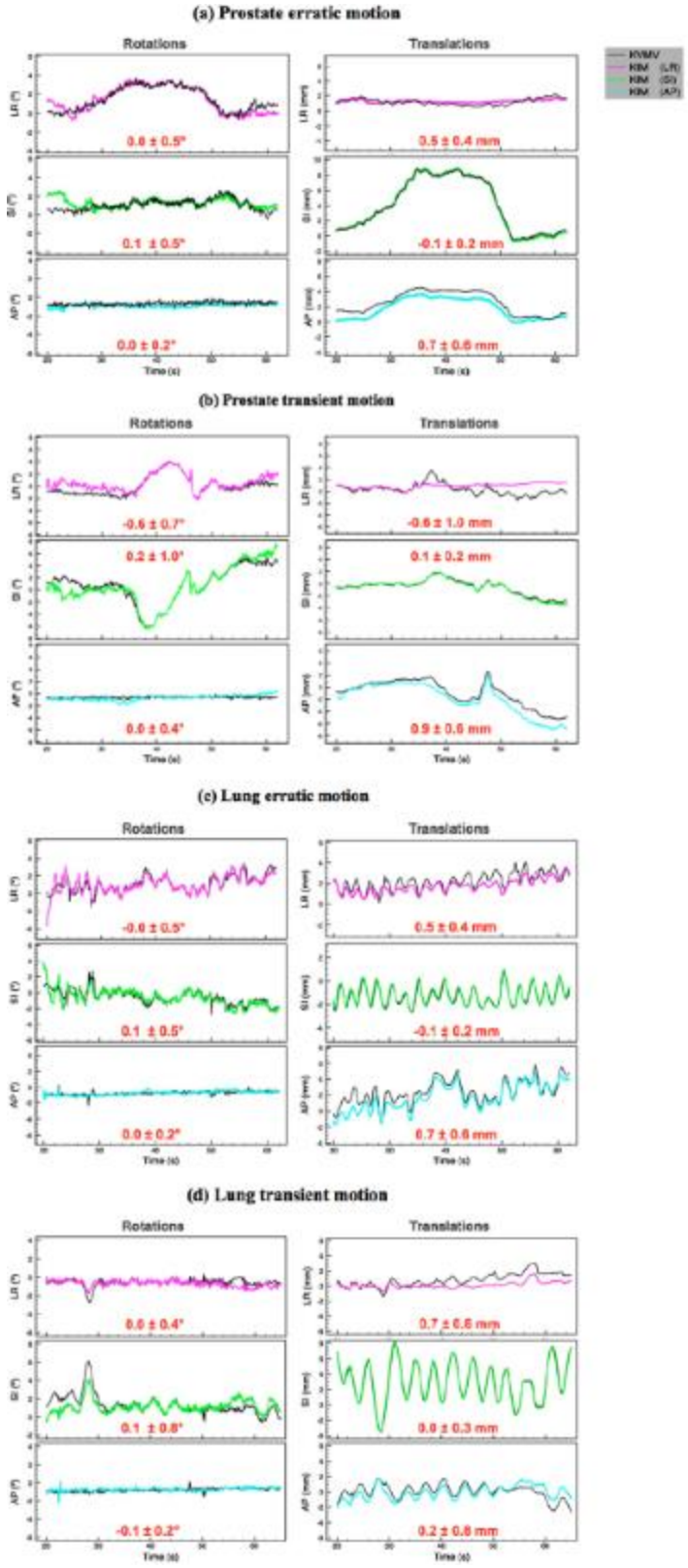

Figure 5. Examples of the time-varying 6 DoF phantom motion measured by KIM (colours) and the corresponding motion derived from kV/MV triangulation (black) for erratic and transient motion trajectories for prostate and lung tumours. Each plot shows 3 rotations (left) and translations (right) with the mean ± s.d differences between the estimated motion and the ground-truth.

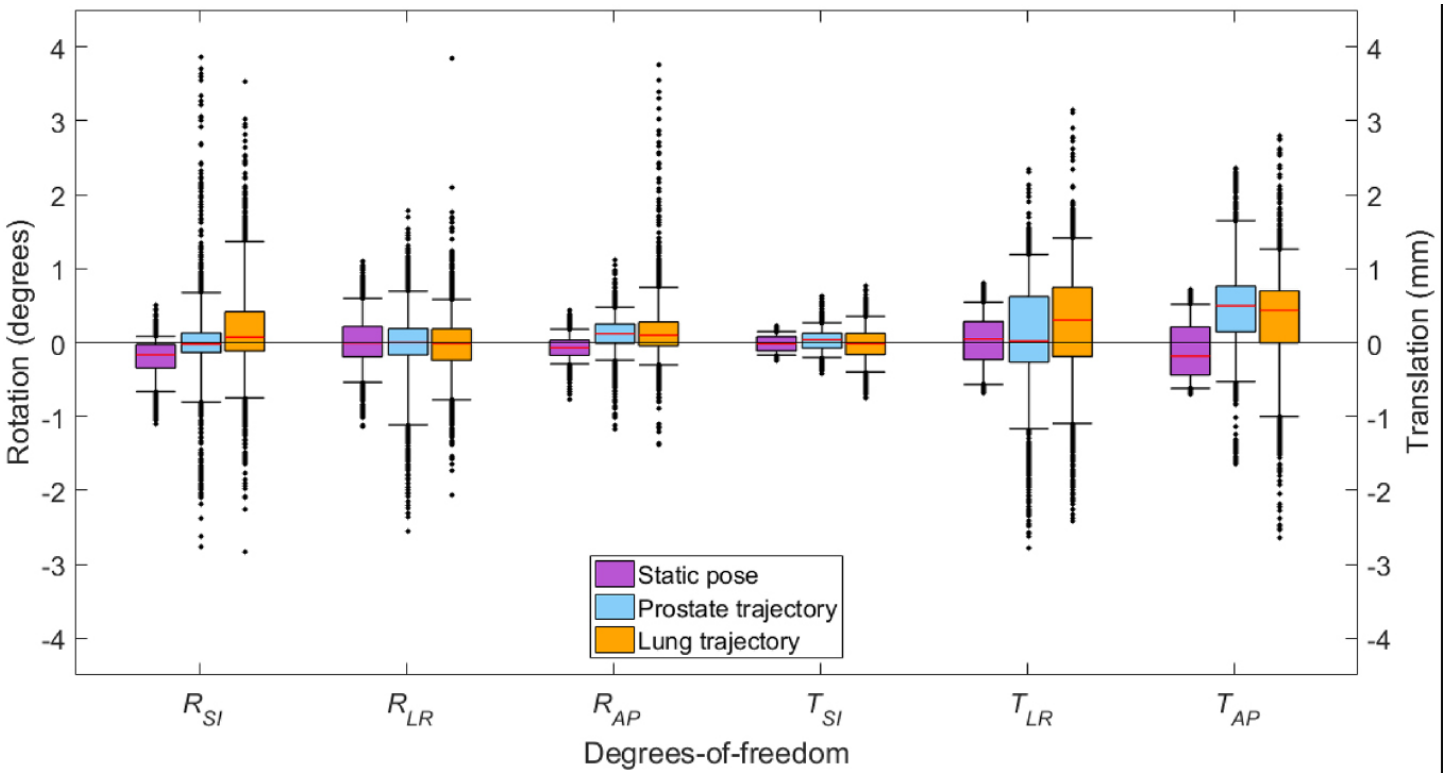

Figure 6. Distribution of the differences in each DoF between KIM and kV/MV derived 6 DoF motions for various motion types. Lower and upper borders of the boxes are the first and third quartiles; lower and upper bars indicate the 5% and 95% percentiles, respectively, and outliers are in symbols. The median (second quartile) is the red bar inside each box.

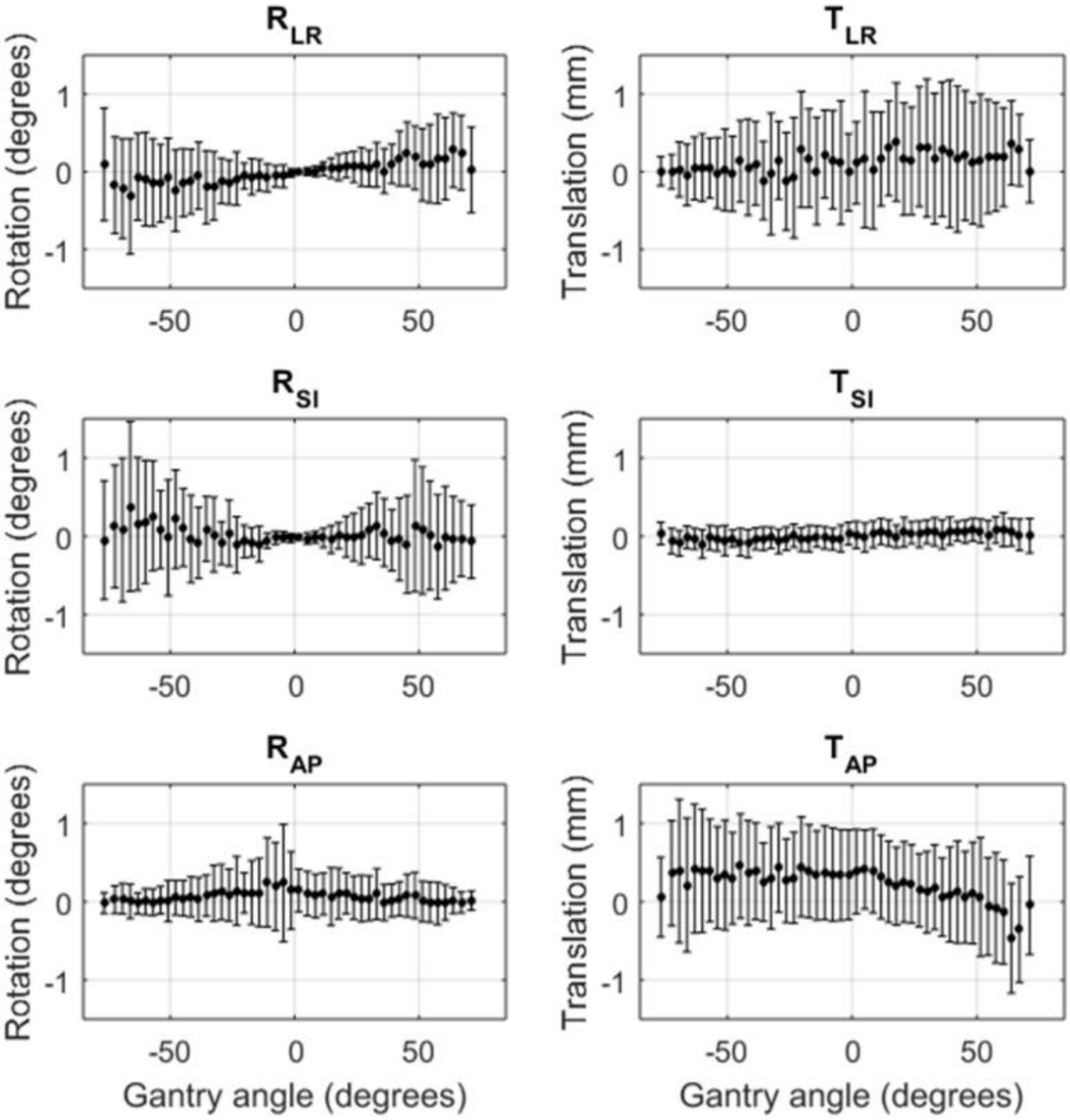

Figure 7. Differences in between 6 DoF KIM and kV/MV triangulation estimated motion as a function of gantry angles. (left) Rotation motion; (right) translation motion. The symbols are mean differences and error bars are 1 s.d.

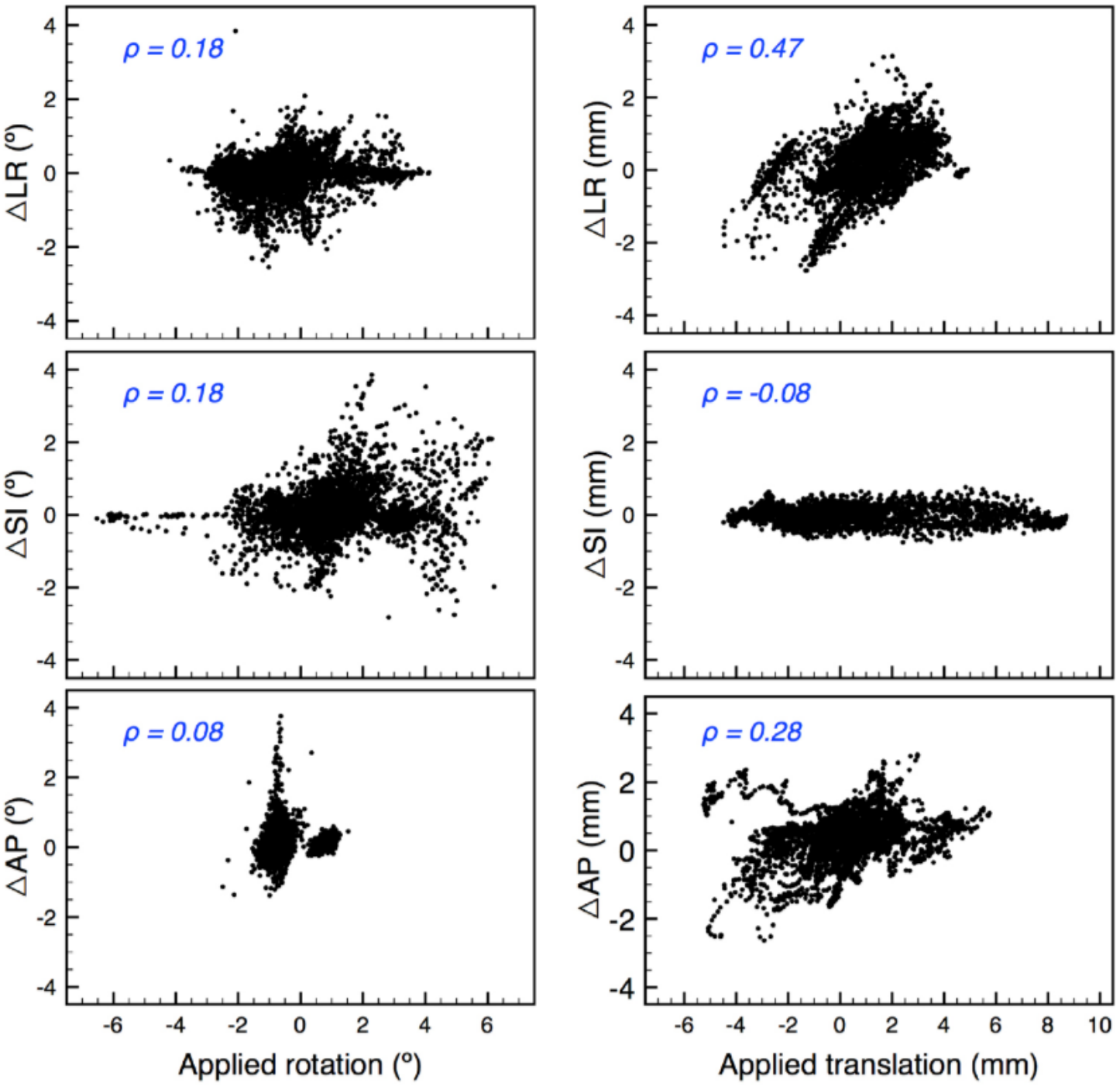

Figure 8. Correlation of the applied motion and the magnitude of error in KIM motion measurements collated from the dynamic motion traces experiments: 3 rotations (left) and 3 translations (right). The Pearson correlation coefficient is displayed on each panel.